# Holographic fabrication of octagon graded photonic super-crystal and potential applications in topological photonics

OLIVER SALE, SAFAA HASSAN, NOAH HURLEY, KHADIJAH ALNASSER, USHA PHILIPOSE, HUALIANG ZHANG, AND YUANKUN LIN 1,3,\*

**Abstract**: Novel optical properties in graded photonic super-crystals can be further explored if new types of graded photonic super-crystals are fabricated. In this paper, we report holographic fabrication of graded photonic super-crystal with eight graded lattice clusters surrounding the central non-gradient lattices through pixel-by-pixel phase engineering in a spatial light modulator. The prospect of applications of octagon graded photonic super-crystal in topological photonics is discussed through photonic band gap engineering and coupled ring resonators.

2D photonic crystal; graded photonic super-crystal; holographic fabrication; photonic band structure

# 1. INTRODUCTION

Diffractive optical element (DOE), such as a phase mask used for the fabrication of fiber Bragg grating, has been a very attractive technique for the holographic fabrication of photonic crystals through one-beam, one DOE and one-exposure method [1,2]. DOE can be used to control the phase profile of a laser beam and generate a desired spatial distribution of the laser intensity. Compared with traditional binary masks, DOE has an advantage of fully using all the incident light power and modulating the light patterns in the beam propagation direction. However, a static DOE cannot be electrically programmed for the control of the laser beam on-the-fly.

A programmable liquid crystal based spatial light modulator (SLM) is a very attractive DOE as it can electronically encode the amplitude or phase of the laser beam in its display of liquid crystal on silicon. The laser beam can be controlled as a tool of dynamic tweezer or micro-rotor [3,4]. The computer-generated hologram displayed in SLM can be used to engineer the phases of interfering for the generation of desired inference patterns with periodic or quasi-periodic, and chiral structures [5-12]. SLMs have been used to fabricate photonic structures with varying lattice orientation, lattice spacing, and filling fraction through innovative synthesis approaches [13-16]. Arbitrary designs of phase patterns were very attractive but they could result in an assignment of several gray levels on a single pixel, consequently leading to a super-lattice effect.

Pixel-by-pixel phase engineering of phase patterns in SLM can produce the highest resolution in the fabricated photonic structure and can also register the desired defects in line with the photonic lattices [17]. Very recently, the pixel-by-pixel phase engineering in checkerboard format in SLM has produced two sets of interfering beams for the fabrication of graded photonic super-crystals (GPSCs) in square lattices where graded lattice clusters formed in square, rectangular, hexagonal and 5-fold symmetries [18-21]. There are three design levels: (a) two gray levels were assigned to the pixels in checkerboard format that produced one set of diffraction spots with a large diffraction angle; (b) two

<sup>&</sup>lt;sup>1</sup>Department of Physics, Univ. of North Texas, Denton, TX 76203, USA

<sup>&</sup>lt;sup>2</sup>ECE Department, University of Massachusetts Lowell, Lowell, MA 01854, USA

<sup>&</sup>lt;sup>3</sup>Department of Electrical Engineering, Univ. of North Texas, Denton, TX 76203, USA

<sup>\*</sup>Corresponding author: yuankun.lin@unt.edu

types of checkerboards with different gray levels fill the pixels alternately in clockwise rotation; (c) the checkerboard fills the unit cell of the phase pattern in square or triangular shape that produced the other set of diffraction spots with a small diffraction angle [18-21]. Single reflective optical element (ROE) has been integrated with SLM for large area fabrication of GPSCs with small feature period [20]. The main advantage of using the pixel-by-pixel phase pattern in checkerboard format in SLM was that the same ROE can be used even when different phase patterns for different graded lattice clusters are designed in SLM [20].

In this paper, octagon GPSCs have been fabricated through 12-beam interference lithography through pixel-by-pixel phase engineering in SLM. The prospect of octagon GPSCs for topological photonics has been discussed in aspects of topological photonic band structures and coupled ring resonators.

#### 2. DESIGN OF PHASE PATTERN IN SLM AND EXPERIMENTAL CONDITIONS

The unit cell of designed phase pattern is shown inside the solid red square in Fig. 1(a). The design of the phase pattern was done by assigning a gray level for each pixel inside the unit cell of  $12 \times 12 = 144$  pixels using the Gimp software. The unit cell is repeated to cover the SLM active area of  $1920 \times 1080$  pixels. The pixel size of the SLM used in this paper is  $8\times8$   $\mu$ m². Thus the SLM has an active area of  $15.36\times8.64$  mm². The unit cell was divided into 8 triangular areas by lines in 0, 45, 90 and 135 degrees relative to x-axis.

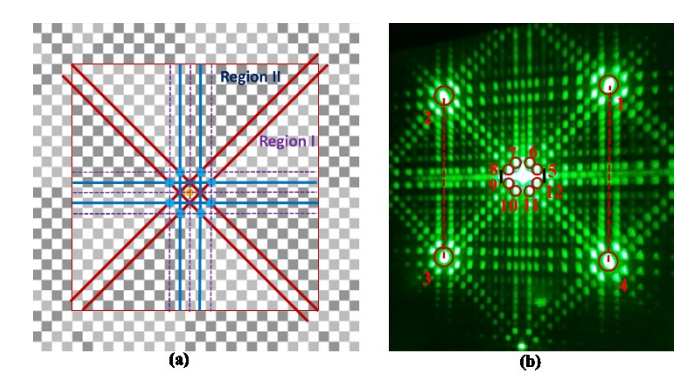


Fig. 1. (a) Designed phase pattern in a unit cell indicated by the solid red square. The pixels were assigned with different gray level pairs in checkerboard format in region (I) and (II). Lines indicate the periodic unit for the diffraction. (b) Optical image of diffraction pattern of 532 nm laser from the phase pattern in SLM. 12 beams, indicated by red circles, pass through the Fourier filter for multi-beam interference. The cell-phone camera was tilted to avoid the back-reflection spots.

The assignment of gray level was based on the diffraction efficiency of formed phase pattern and simulation of iso-intensity of interference pattern using these efficiencies for the formation of GPSC [18,19]. Gray levels of (184, 254) were used for the assignment of gray levels in checkerboard format for pixels in region I inside the unit cell in Fig. 1(a) while (128,254) were used for region II inside the unit cell in Fig. 1(a). The checkerboard patterns in regions (I) and (II) were used to alternately fill 8 areas in the whole unit cell in counter clockwise direction. The pixels between two checkerboard formats (along the red lines in Fig. 1(a)) were filled in a way such that a half of pixels were filled with a grey level of 184 and the other half of pixels were filled with 128 as seen along the solid red lines

and central dashed purple lines. The gamma curve will apply a phase of  $0\pi$  into a gray level of 0 and  $2\pi$  phase into a gray level of 255 when the laser beam was incident onto the phase pattern in the SLM. In general, we can assume the phase is gray level× $2\pi/255$  although the gamma curve is not a perfect linear line in the whole range. We generally avoid using the gray level of 255 because 255 might be explained as  $2\pi$  or  $0\pi$  in phase.

Figure 1(b) shows an optical image of diffraction pattern (taken with a cell-phone) when a 532 nm laser is incident onto the phase pattern in the SLM. The camera was tilted to avoid the back-reflection spots. The first order diffraction efficiency can be optimized following the measured efficiency as a function of gray level differences [18,19]. However, the appearance of other order diffractions in Fig. 1(b) helped to identify the origin of diffractions due to the pattern in Fig. 1(a). The diffraction spots labelled by 1, 2, 3 and 4 in Fig. 1(b) are due to the diffraction from periodic arrangement of two gray level array such as (184,254) in region I in Fig. 1(a) through a Bragg diffraction (2 pixels)×sin  $(\theta_1)=m\lambda$ , where  $\theta_1$  is the diffraction angle as defined in Fig. 2 and m is an integral number. Pair of diffraction spots (6,7), (8,9), (10,11) and (12,6) are in Fig. 1(b) are due to the diffraction from periodic arrangement of 24 pixels as indicated by the horizontal or vertical lines in Fig. 1(a) through Bragg equation (24 pixels)×sin  $(\theta_2)=\lambda$ , where  $\theta_2$  is the diffraction angle as defined in Fig. 2. The distance d(2,3) between spot 2 and 3 in Fig. 1(b) is D(2,3)= $2 \times f_1 \times \tan(\theta_1)$  and the distance d(8, 9) between spot 8 and 9 is  $D(8,9)=2\times f_1\times \tan(\theta_2)$ . The ratio of  $d(2,3)/d(8,9)\approx 12$ . Because of titled image in Fig 1(b), the experimental value can be measured by the average of d(2,3) and d(1,4) over the average of d(8,9) and d(5,12), which is 11.9. There are also strong diffractions in diagonal directions in Fig. 1(b) due to periodic array of pixels indicated by the solid red lines in Fig. 1(a). The overlap of diffraction in vertical (horizontal) and diagonal directions, as indicated by the solid blue (blue) and solid red lines in Fig. 1(a), respectively, can help determine the azimuthal angle  $\gamma$  for beam 5 in Fig. 1(b) which can be calculated by  $\gamma$ =atan(1/2)=26.57 degrees relative to x-axis. The measured value for the angle in Fig. 1(b) for beam 5 is 26.6 degrees. The azimuthal angles for beams 6-12 are assigned to be  $90-\gamma$ ,  $90+\gamma$ ,  $180-\gamma$ ,  $180+\gamma$ ,  $270-\gamma$ ,  $270+\gamma$ , and  $360-\gamma$ , respectively. The size change of the square unit cell in the phase pattern will not change the azimuthal angles of these 12 beams. However, such a change can lead to octagon GPSCs with a different unit super-cell size for device applications.

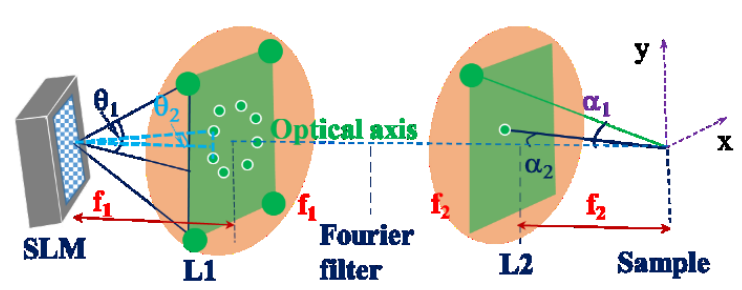


Fig. 2. Schematic of the optical setup for the holographic fabrication of octagon GPSC. The diffracted beams from the phase pattern displayed in SLM are filtered at the Fourier Plane and form interference patterns through 4f imaging system.  $\theta_1$  and  $\theta_2$  are the first order diffraction angles due to the periodic array of 2 pixels, 24 pixels, respectively.  $\alpha_1$  and  $\alpha_2$  (zenith angle) are the interfering angles of 1-4 beams and 5-12 beams in Fig. 1(b), respectively.

Figure 2 shows the optical setup for the holographic fabrication of GPSCs. A laser beam with a wavelength of 532 nm (Cobolt Samba 50 mW) was expanded and collimated by using a spatial filter and lens. The laser's polarization is along the longer side of SLM and is incident with an incident angle of 4 degrees. The laser beam was modulated in phase by the phase pattern displayed in the SLM (Holoeye PLUTO). The diffraction spots from the phase pattern are collected through lens1 and filtered by a Fourier filter at the Fourier plane so that only beams 1-12 in Fig. 1(b) can pass through. 4f imaging system was used with a focal length of  $f_1$ =400 mm and  $f_2$ = 200 mm for lens 1 and lens 2, respectively. The 12 beams were overlapped through lens 2 and exposed to a photo sensitive mixtures of dipentaerythritol penta/hexaacrylate (DPHPA) monomer, photo initiator rose bengal, co-initiator N-phenyl glycine (NPG), and chain extender N-vinyl pyrrolidinone (NVP) [18]. The mixture was spin-coated on a glass slide with a speed of 2500 rpm for 30 seconds. The GPSC sample was developed in PGMEA for 5 minutes, rinsed by isopropanol for 1 minute and then dried.

# 3. MULTI-BEAM INTERFERENCE LITHOGRAPHY AND RESULTS

The intensity I(r) of 12 beam interference can be described by Eq. (1):

$$I(r) = \langle \sum_{i=1}^{12} E_i^2(r,t) \rangle + \sum_{i< j}^{12} E_i E_j \hat{e}_i \cdot \hat{e}_j cos[(k_j - k_i) \cdot r + (\delta_j - \delta_i)]. \tag{1}$$

where E, k,  $\delta$ , E, e are the electric field amplitude, the wave vector, the initial phase, and the electric field polarization direction, respectively.

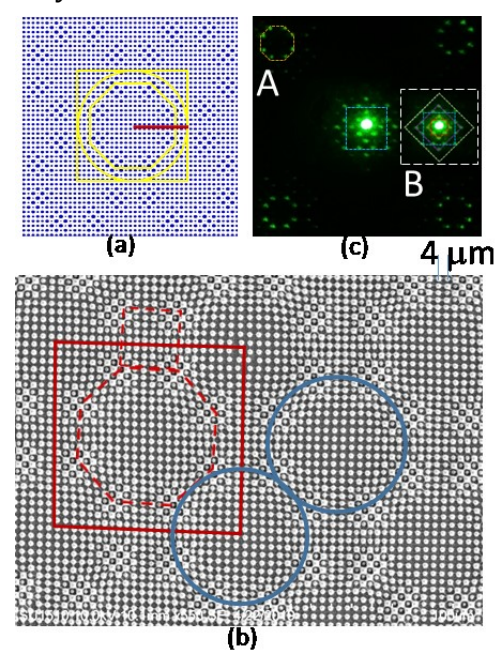


Fig. 3. (a) Simulated 12-beam interference pattern with 8 graded regions forming octagon and surrounding the central almost uniform region. The yellow square indicates the unit super-cell. (b) SEM image of a fabricated sample where the 8 graded regions are connected by a dashed red octagon. The solid red square indicates the unit super-cell and both squares indicate a square symmetry. A lattice spacing parameter  $\Lambda$ =4  $\mu$ m. (c) Diffraction pattern of fabricated sample from 532 nm laser. The yellow octagon connecting the 8 diffraction spots at the location A is for eye guidance. An insert inside the dashed white square at the

location B is a copy of pattern in the central region. The five squares inside the dashed white square is for eye guidance purpose.

The wavevectors for beams 1-4 can be described as  $k(\sin(\alpha_1)\cos(O_{1-4}), \sin(\alpha_1)\sin(O_{1-4}), \cos(\alpha_1))$ , where the angle O<sub>1-4</sub> is 45, 135, 225, and 315 degrees, respectively. The wavevectors for beams 5-12 can be described by  $k(\sin(\alpha_2)\cos(I_{5-12}), \sin(\alpha_2)\sin(I_{5-12}), \cos(\alpha_2))$ , where the angle  $I_{5-12}$  is  $\gamma$ , 90– $\gamma$ , 90+ $\gamma$ , 180– $\gamma$ , 180+ $\gamma$ , 270– $\gamma$ , 270+ $\gamma$ , and 360- $\gamma$ , respectively. Using Eq. (1), the interference intensity is calculated and shown in Fig. 3(a). The interference pattern has a large size of unit supercell as indicated by the yellow square. Because the interfering angle  $\alpha_1$  is much larger than  $\alpha_2$ , the interference pattern can approximately be understood as 1-4 beam interference with a small feature, modulated by 5-12 beam interference with a large feature. The interference among 1-4 produce lattices with a lattice constant= $2\pi/(k \sin(\alpha_1))((\cos(45) \cos(135))=\lambda/(\sqrt{2}\sin a_1)$ , where  $\alpha_1=\theta_1\times f_1\times\sqrt{2}/f_2$ . Thus the lattice constant  $\Lambda$  equals pixel-sidelength/2=4 um. The modulation of 1-4 beam interference in radial direction by the 5-12 beams can be characterized by a radius of a yellow circle in Fig. 3(a). The set of  $(k_n - k_{n+2})$  among 5-12 beams forms a circle . for example,  $(k_5-k_7)=k\times\sin(\alpha_2)\times(2\sin(\gamma+45)\sin(45), -2\cos(\gamma+45)\sin(45), 0)$ . The generated interference forms a modulation circle with a radius= $2\pi/(k \sin(\alpha z))$  $\sqrt{2} = \lambda/(\sqrt{2} \sin a_2) = 24$  pixel-side-length/4=48 µm=12 $\Lambda$ , as shown by the red bar in Fig. 3(a). The sold yellow square in Fig. 3(a) has the unit super-cell size of 12 $\Lambda$ ×12 $\Lambda$ . There are 8 graded regions surrounding the central almost-uniform region as indicated by the yellow octagon in Fig. 3(a). When the number of side graded regions increases, these graded regions form super-cavity or the central almost-uniform region forms the cavity core in the hetero-structure photonic crystal [22].

Fig. 3(b) shows the SEM image of fabricated GPSC in DPHPA mixture. The lattice constant  $\Lambda$ =4  $\mu$ m as measured in SEM. The photonic band structure can predict the operating frequency  $a/\lambda$  where  $\lambda$ is the operating wavelength. Thus  $\lambda$  is scalable with the lattice constant a. The lattice constant a can be further reduced by the 4f imaging system or by integrating an reflective optical element with the SLM [20] in order to achieve the desired operating wavelength. The red square indicates the unit super-cell of  $12\Lambda \times 12\Lambda$ . The 8 graded regions are connected by the dashed red octagon. The fabricated sample matches the simulated interference pattern. A square symmetry is obvious as seen from the unit super-cell and the dashed red square connecting 4 graded region at the unit super-cell boundary in Fig. 3(b). The square symmetry is also confirmed in the diffraction pattern of fabricated sample by 532 nm laser, as shown in Fig. 3(c). The insert inside the dashed white square at the location B is the copy of the diffraction pattern from the central region but with drawing of squares connecting the diffraction spots. We have used five squares in the insert to connect all spots, indicating the order of modulated lattices in fabricated sample. There are four diffraction regions at the each corner of the square in Fig. 3(c). One of them is indicated by the dashed yellow octagon at the location A. These spots contain the lattice information in the unit super-cell. The octagon diffraction in Fig. 3(c) spots correspond to 8 graded regions inside the unit super-cell in Fig. 3(b).

# 4. DISCUSSION: prospect in applications in topological photonics

If silicon (dielectric constant=12) is used in the GPSCs, the graded regions have several photonic band gaps while the central almost-uniform region has one photonic band gap [24]. There is no band gap in the boundary of the graded and uniform regions in certain frequency range due to the

dislocation of photonic band gap in either sides. Fig. 4(a) and 4(b) show simulated E-field distribution in the octagon GPSCs following the method in the reference [18]. These E-fields appear in the boundary at a frequency  $a/\lambda=0.410$  and 0.409 in Fig. 4(a) and 4(b), respectively. Usually the appearance of interface states are characteristic of topological photonics [25]. Further design at pixel levels in the phase pattern in SLM can be added into the square unit cell of the phase pattern for the generation of photonic structures with desired photonic band structures for the interface states [16-17].

The photonic band structure can also be engineered so that the E-fields are confined in the graded regions and coupled to form ring resonances as a side ring among the 8 graded region and as a link ring among the 4 graded regions as shown in Fig. 3(b), Fig. 4(b) and Fig. 4(c) for applications in topological photonics [26,27].

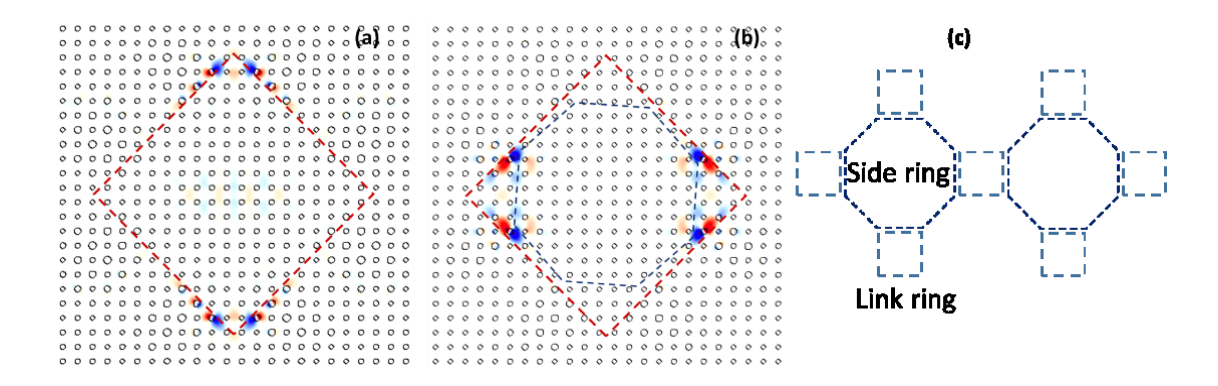


Fig. 4. (a-b) Simulated electric field distributions in the boundary of graded and uniform regions. (c) Possible side and link ring formation in octagon GPSCs.

### 5. CONCLUSION

In this paper, we have fabricated octagon GPSCs through holographic lithography via a simple pixel-by-pixel phase design in a square unit cell of phase pattern displayed in the digital SLM. The prospect of octagon GPSCs for topological photonics has been discussed.

Funding Information. National Science Foundation (NSF) (1661842 and 1661749)

### References

- 1. Chanda D, Abolghasemi L, Haque M, Ng M, Herman P. Multi-level Diffractive Optics for Single Laser Exposure Fabrication of Telecom-Band Diamond-like 3-Dimensional Photonic Crystals. Opt. Express, 2008, 16: 15402-15414.
- 2. Ohlinger K, Zhang H, Lin Y, Xu D, and Chen K. A tunable three layer phase mask for single laser exposure 3D photonic crystal generations: bandgap simulation and holographic fabrication. Opt. Mater. Express, 2011, 1: 1034-1039.
- 3. Leach J, Wulff K, Sinclair G, Jordan P, Courtial J, Thomson L, Gibson G, Karunwi K, Cooper J, Laczik Z, and Padgett M. Interactive approach to optical tweezers control. Appl. Opt., 2006, 45: 897-903.
- 4. Xavier J, Dasgupta R, Ahlawat S, Joseph J, and Gupta P. Three Dimensional Optical Twisters-driven Helically-Stacked Multi-layered Microrotors. Appl. Phys. Lett., 2012, 100: 121101.

- 5. Zito G, Piccirillo B, Santamato E, Marino A, Tkachenko V, and Abbate G. Two-dimensional photonic quasicrystals by single beam computer-generated holography. Opt. Express, 2008, 16: 5164-5170.
- 6. Jenness N, Wulff K, Johannes M, Padgett M, Cole D, and Clark R. Three-dimensional parallel holographic micropatterning using a spatial light modulator. Opt. Express, 2008, 16: 15942-15948.
- 7. Arrizón V, Sánchez de-la-Llave D, Méndez G, and Ruiz U. Efficient generation of periodic and quasi-periodic non-diffractive optical fields with phase holograms. Opt. Express, 2011, 19: 10553-10562.
- 8. Xavier J, Rose P, Terhalle B, Joseph J, and Denz C. Three-dimensional optically induced reconfigurable photorefractive nonlinear photonic lattices. Opt. Lett., 2009, 34: 2625-2627.
- 9. Xavier J, and Joseph J. Tunable Complex Photonic Chiral Lattices by Reconfigurable Optical Phase Engineering. Opt. Lett., 2011, 36: 403-405.
- 10. Xavier J, Vyas S, Senthilkumaran P, Denz C, and Joseph J. Sculptured 3D twister superlattices embedded with tunable vortex spirals. Opt. Lett., 2011, 36: 3512-3514.
- 11. Behera S, and Joseph J. Single-step optical realization of bio-inspired dual-periodic motheye and gradient-index-array photonic structures. Opt. Lett., 2016, **41**: 3579.
- 12. Lutkenhaus J, George D, Moazzezi M, Philipose U, and Lin Y. Digitally tunable holographic lithography using a spatial light modulator as a programmable phase mask. Opt. Express, 2013, 21: 26227-26235.
- 13. Kumar M, and Joseph J. Optical generation of a spatially variant two-dimensional lattice structure by using a phase only spatial light modulator. Appl. Phys. Lett., 2014, **105**: 051102.
- 14. Rumpf R, and Pazos J. Synthesis of spatially variant lattices. Opt. Express, 2012, 20: 15263–15274.
- 15. Digaum J, Pazos J, Chiles J, D'Archangel J, Padilla G, Tatulian A, Rumpf R, Fathpour S, Boreman G, and Kuebler S. Tight Control of Light Beams in Photonic Crystals with Spatially-Variant Lattice Orientation. Opt. Express, 2014, 22: 25788-25804.
- 16. Lutkenhaus J, George D, Lowell D, Arigong B, Zhang H, and Lin Y. Registering functional defects into periodic holographic structures. Applied Optics, 2015, 54: 7007.
- 17. Lutkenhaus J, Lowell D, George D, Zhang H, and Lin Y. Holographic Fabrication of Designed Functional Defect Lines in Photonic Crystal Lattice Using a Spatial Light Modulator. Micromachines, 2016, 7:59.
- 18. Lowell D, Lutkenhaus J, George D, Philipose U, Chen B, and Lin Y. Simultaneous direct holographic fabrication of photonic cavity and graded photonic lattice with dual periodicity, dual basis, and dual symmetry. Opt. Express, 2017, 25: 14444.
- 19. Lowell D, Hassan S, Sale O, Adewole M, Hurley N, Philipose U, Chen B, and Lin Y. Holographic fabrication of graded photonic super-quasi-crystal with multiple level gradients, Applied Optics, 2018, 57: 6598.
- 20. Lowell D, Hassan S, Adewole M, Philipose U, Chen B, and Lin Y. Holographic fabrication of graded photonic super-crystals using an integrated spatial light modulator and reflective optical element laser projection system. Appl. Opt., 2017, 56: 9888.
- 21. Hassan S, Sale O, Lowell D, Hurley N, and Lin Y. Holographic fabrication and optical property of graded photonic super-crystals with a rectangular unit super-cell. Photonics, 2018, 5: 34.

- 22. Ge X, Minkov M, Fan S, Li X, and Zhou W. Low index contrast heterostructure photonic crystal cavities with high quality factors and vertical radiation coupling. Appl. Phys. Lett., 2018, 112: 141105.
- 23. Hassan S, Lowell D, and Lin Y. High light extraction efficiency in organic light-emitting diodes by patterning the cathode in graded superlattice with dual periodicity and dual basis. J. Appl. Phys., 2017, 121: 233104.
- 24. Hassan S, Alnasser K, and Lin Y. Effects of Photonic Band Structure and Unit Super-Cell Size in Graded Photonic Super-Crystal on Broadband Light Absorption in Silicon. Photonics, 2019, 6: 50.
- 25. Lu L, Joannopoulos J, and Soljačić M. Topological photonics. Nature Photonics, 2014, 8: 821.
- 26. Bandres M, Wittek S, Harari G, Parto M, Ren J, Segev M, Christodoulides D, Khajavikha M. Topological insulator laser: Experiments. *Science*, *2018*, 359: eaar4005.
- 27. Ao Y, Hu X, Li C, You Y, and Gong Q. Topological properties of coupled resonator array based on accurate band structure. Phys. Rev. Mat., 2018, 2: 105201.